

Copyright is owned by the Author of the thesis. Permission is given for a copy to be downloaded by an individual for the purpose of research and private study only. The thesis may not be reproduced elsewhere without the permission of the Author.

Approaches to forecast volcanic hazard in the Auckland Volcanic Field, New Zealand

A thesis presented in partial fulfilment of the requirements for the
degree of Doctor of Philosophy in Earth Science

At Massey University, Palmerston North, New Zealand



MASSEY UNIVERSITY
TE KUNENGA KI PŪREHUROA
UNIVERSITY OF NEW ZEALAND

Gabor Kereszturi

2014

No Telling Where Next

But Signs Expected

When any of the 50 volcanic centres in Auckland next erupts, there is likely to be some warning to allow evacuation.

"Unlike with earthquakes, it is possible to see something coming," the senior lecturer in geology at the University of Auckland, Dr Ian Smith, told a civil defence seminar yesterday.

The next eruption could occur anywhere in metropolitan Auckland, but it was likely to be of short duration.

The last eruption to affect people in New Zealand was Tarawera, 100 years ago.

Dr Smith said yesterday: "What we need in this country is a good eruption to remind people about the effects it can have."

Auckland University has established a seismometer on Motutapu Island and the Auckland Regional Authority is siting others at dams in the Hunua and Waitakere ranges.

Dr Smith said these would give between 24 hours and a week's

warning of coming volcanic activity.

The threat to life would not be great but destruction of property could be considerable.

The last local eruption was on Rangitoto about 800 years ago.

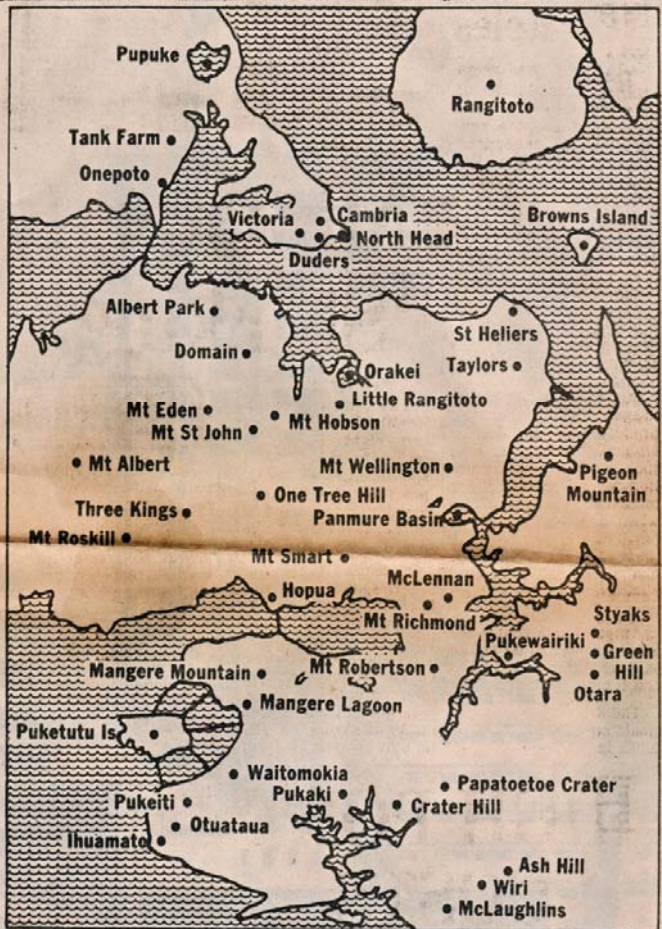
Explosive outbursts could be expected from areas like the Orakei or Panmure basins, Lake Pupuke or the Onepoto basin.

The blasts would cause destruction up to three kilometres away with damage extending several kilometres. Such eruptions had produced 160 km/h surges, removing trees for up to a kilometre.

In addition, wet ash would clog drains, affect water supplies and disrupt traffic. The weight of it could cause buildings to collapse.

The more visible cones such as Mt Eden, Mt Wellington or Mangere could throw up lava, producing heat damage up to a kilometre away.

Dr Smith said that there was no way of predicting where a future eruption would be.



The main volcanic areas in Auckland.

Abstract

Monogenetic basaltic volcanism is characterised by a complex array of behaviours in the spatial distribution of magma output and also temporal variability in magma flux and eruptive frequency. For understanding monogenetic volcanoes different topographic and remote sensing-based information can be used, such as Digital Surface Models (DSMs). These data are most appropriately analysed in a Geographic Information System (GIS). In this study a systematic dataset of the Auckland Volcanic Field (AVF), New Zealand, was collected and pre-processed to extract quantitative parameters, such as eruptive volumes, sedimentary unit thicknesses, areas affected, spatial locations, and topographic positions. The topographic datasets available for the AVF were Shuttle Radar Topography Mission (SRTM), Advanced Spaceborne Thermal Emission and Reflection Radiometer (ASTER), contour-based Digital Elevation Models, and Light Detection And Range (LiDAR) datasets. These were validated by comparing their elevations to high accuracy ground control reference data from multiple Real-Time-Kinematic (RTK) Global Positioning System and Terrestrial Laser Scanning surveys. The attribute extraction was carried out on the LiDAR DSM, which had the best vertical accuracy of ≤ 0.3 m. The parameterisation of monogenetic volcanoes and their eruptive products included the extraction of eruptive volumes, areas covered by deposits, identification of eruptive styles based on their sedimentary characteristics and landform geomorphology. A new conceptual model for components of a monogenetic volcanic field was developed for standardising eruptive volume calculations and tested at the AVF. In this model, a monogenetic volcano is categorised in six parts, including diatremes beneath phreatomagmatic volcanoes, or crater infills, scoria/spatter cones, tephra rings and lava flows. The most conservative estimate of the total Dense Rock Equivalent eruptive volume for the AVF is 1.704 km^3 . The temporal-volumetric evolution of the AVF is characterised by a higher magma flux over the last 40 ky, which may have been triggered by plate tectonic processes (e.g. increased asthenospheric shearing and back-arc spreading underneath the Auckland region). The eruptive volumes were correlated with the sequences of eruption styles preserved in the pyroclastic record, and environmental influencing factors, such as distribution and thickness of water-saturated post-Waitemata sediments, topographic position, distance from the sea and known fault lines. The past eruptive sequences are characterised by a large scatter without any initially obvious trend in relation to any of the four influencing factors. The influencing factors, however, showed distinct differences between sub-domains of the field, i.e. North Shore, Central Auckland and Manukau Lowlands. Based on the spatial variability of these environmental factors, a susceptibility conceptual model was provided for the AVF. Based on the comparison of area affected by eruption styles and eruptive volume, lava flow inundation is the most widespread hazard of the field. To account for this, a topographically adaptive numerical method was developed to model the susceptibility for lava flow inundation in the AVF. This approach distinguished two different hazard profiles for the valley-dominated Central Auckland and North Shore regions, and the flat Manukau Lowlands. A numerical lava flow simulation code, MAGFLOW, was applied to understand the eruption and rheological properties of the past AVF lava flow in the Central Auckland area. Based on the

simulation of past lava flows, three eruptive volume-based effusive eruption scenarios were developed that best characterise the range of hazards expected.

To synthesise, susceptibility mapping was carried out to reveal the patterns in expected future eruption styles of the AVF, based on the eruptive volumes and environmental factors. Based on the susceptibility map, the AVF was classified as highly susceptible to phreatomagmatic vent-opening eruptions caused by external environmental factors. This susceptibility map was further combined with eruptive volumes of past phreatomagmatic phases in order to provide an eruption sequence forecasting technique for monogenetic volcanic fields. Combining numerical methods with conceptual models is a new potential direction for producing the next generation of volcanic hazard and susceptibility maps in monogenetic volcanic fields. These maps could improve and standardise hazard assessment of monogenetic volcanic fields, raising the preparedness for future volcanic unrest.

Acknowledgements

I would like to express my great thanks for the many people whom I have interacted in the last few years, and who helped me to complete my PhD thesis. First of all, I am thankful to my chief-supervisors, Károly Németh and Jonathan Procter, for guiding me through the PhD process. I am also thankful for the contributions from my co-supervisors, Shane J. Cronin, Jan M. Lindsay (University of Auckland, New Zealand), Mike Tuohy, Mark Bebbington and Győző Jordán (Hungarian Academy of Science, Hungary). Many thanks to Kate Arentsen for helping me to improve the presentation of this thesis. Special thanks go to all the staff and students of the Volcanic Risk Solutions group at Massey University, for their support and help my PhD studies, including Javier Agustin-Flores, Kate Arentsen, Eric Breard, Marco Brenna, Magret Damaschke, Gaby Gomez, Matt Irwin, Emily Kawabata, Gert Lube, Anja Möbis, Adam Neather, Natalia Pardo, Bob Stewart, Rafael Torres-Orozco, Manuela Tost, Georg Zellmer, Anke Zernack and Ting Wang.

For financial help, I would like to thank the Institute of Agriculture and Environment at Massey University for the PhD Research Fellowship. This work was also supported by the Massey University-led FRST-IIOF project “Facing the challenge of Auckland’s volcanism” and the Natural Hazards Research Platform project “Living with Volcanic Risk”, based at Massey University, as well as the DEtermining VOlcanic Risk in Auckland (DEVORA) project, co-funded by the NZ Earthquake Commission (EQC) and the Auckland Council, GNS Science, University of Auckland and Massey University.

I am thankful for the use of LiDAR data, which was provided by Auckland Council. I would also like to thank Tracy Howe, Elaine Smid and Madison Frank (University of Auckland) for their help in requesting the LiDAR data. Special help with the LiDAR dataset and details of its “origin” were given by Carl Ellaway (Auckland Council), Michael De Lacy (Fugro Spatial, Australia) and Jeremy Neilson (NZ Aerial Mapping Ltd). During the GPS and Terrestrial Laser Scanning surveys the important help of Bruce Robinson and Simon Smith (Global Survey, Auckland) was appreciated. In the field and the laboratory, many people have helped me including Anja Möbis, Javier Agustin-Flores, Jonathan Procter, Károly Németh, Hugo Murcia, Jan M. Lindsay, Natalia Pardo, Lucy McGee and Katarina Postekova. Their patience and support are appreciated, especially when they helped me to carry heavy equipment over long-distances. Thank you also to the Department of Conservation/Te Papa Atawhai who helped many times with logistics of field work on Browns Island. During the lava flow modelling, I am grateful for the help of Annalisa Cappello, Gaetana Ganci, Ciro Del Negro, Giuseppe Bilotta and Alexis Hérault (Istituto Nazionale di Geofisica e Vulcanologia, Catania, Italy). They made my stay in Catania wonderful and scientifically fruitful. Financial aid for this visit was made possible through the DEVORA project.

I am grateful to Győző Jordán for encouraging me to pursue research in the field of remote sensing and Geographical Information System (GIS). My former supervisors, György Less, János Földessy and Éva Hartai (University of Miskolc, Hungary), are thanked for supporting me to continue my PhD studies at Massey University in New Zealand.

For the “Thursdays”, I am really thankful to those people who made my stay in Palmerston North beautiful, including Marcela Humphrey, Natalia Pardo, Javier Agustin-Flores, Adimar Lujan, Jimena Rodríguez, Thiago Alves Amaro, Rafael Torres-Orozco, Ana Mar-Sarabia, Gaby Gómez, Hatim El Al, Marco Brenna, Friederike von Schlippe and Daniel Farley.

I wish to thank my parents in Hungary for their support and encouragement throughout my PhD study.

I owe the biggest thanks in the world to my loving wife, Angela, who has supported me over this intense period of my life. Thank you very much for being with me.

Table of Contents

Abstract	i
Acknowledgements.....	iii
Table of Contents.....	v
List of Figures.....	ix
List of Tables.....	xix
Chapter One – Introduction.....	3
1.1. Monogenetic volcanoes and their hazards.....	3
1.2. GIS and remote sensing of monogenetic volcanoes	6
1.3. Aims and objectives	9
1.4. Thesis outline and structure.....	10
Chapter Two – Geological setting	15
2.1. Introduction	15
2.2. Basement geology of Auckland.....	15
2.3. Basaltic monogenetic volcanism in Auckland.....	20
2.3.1. Quaternary basaltic volcanism in the North Island.....	20
2.3.2. Melt extraction models and geochemical evolution.....	22
2.3.3. Eruption styles and volcanic landforms	25
2.3.4. Volcanic hazard assessment and monitoring system	30
Chapter Three – Materials and methods	39
3.1. Introduction to Digital Terrain Analysis (DTA).....	39
3.2. Materials and methods	41
3.2.1. Input data types available in Auckland	41
3.2.2. Data acquisition and pre-processing	47
3.2.3. Data interpolation.....	51
3.2.4. Post-processing techniques.....	56
3.2.5. Testing topographic datasets for Auckland	57
3.2.5.1. Terrain height and representation.....	58
3.2.5.2. Terrain attributes in 2D and 3D	59
3.3. Results: accuracy and variability	64
3.4. Which input data should be used?	72
Chapter Four – Quantitative parameterization of monogenetic volcanoes: geometry and volumes	82
4.1. Introduction	82
4.2. Model for volume estimates of monogenetic volcanoes.....	84
4.2.1. Bulk subsurface volume	86
4.2.2. Bulk proximal tephra accumulation and lava flows volume	88
4.2.3. Bulk medial to distal pyroclastic volume	90
4.3. Input data and configuration for the AVF	92
4.3.1. Bulk subsurface volume for the AVF	92
4.3.2. Bulk proximal tephra accumulation and lava flows volumes for the AVF	93
4.3.3. Bulk medial to distal pyroclastic volume for the AVF	95
4.4. Converting bulk to Dense Rock Equivalent (DRE) eruptive volumes	96

4.5. Results	101
4.6. Discussion.....	107
4.6.1. Limits and errors in eruptive volume estimates	107
4.6.2. Spatial and temporal magma flux.....	108
4.6.3. Integrating eruptive volumes with the AVF's evolution.....	110
4.6.4. AVF evolution and relationship to neighbouring fields	115
4.6.5. Volcanic hazard consequences.....	115
4.7. Conclusions.....	116
 Chapter Five – Linking eruptive volumes to eruptive styles.....	 121
5.1. Introduction.....	121
5.2. Methodology and conceptual framework.....	122
5.2.1. Coding of eruption styles and their eruptive volumes.....	122
5.2.2. Defining area affected in an eruptive history.....	131
5.2.3. Influencing factors on eruption styles	132
5.3. Results	135
5.3.1. Types and distribution of past eruptive histories	135
5.3.2. Influences on AVF eruptive sequences	141
5.4. Discussion.....	144
5.4.1. Factors influencing eruption style	144
5.4.2. A spatial model for distribution of factors influencing eruption style	145
5.5. Conclusion	148
 Chapter Six – Lava flow susceptibility mapping.....	 154
6.1. Introduction.....	154
6.2. Materials and methods.....	157
6.2.1. LiDAR survey and DSM preparation.....	157
6.2.2. Lava flow parameters	158
6.2.3. Hydrological channel extraction	162
6.2.4. Topographic classification of zones subject to lava flow inundation	163
6.2.5. Watershed characteristics	167
6.3. Results	168
6.3.1. Characteristics of past lava flows.....	168
6.3.2. Characteristics of present topography	170
6.4. Discussion.....	173
6.4.1. Lava flow susceptibility.....	178
6.4.2. Watershed characteristics	179
6.4.3. Evaluation of the method and its limitations	181
6.6. Conclusions.....	183
 Chapter Seven – Effusive eruption scenarios based on lava flow simulations	 189
7.1. Introduction.....	189
7.2. Materials and methods.....	194
7.2.1. MAGFLOW code.....	194
7.2.2. Input data for simulation of past lava flows	197
7.2.3. Matching lava flows with simulation results	200
7.3. Results	200
7.4. Discussion.....	206
7.4.1. Volume-limited versus cooling-limited flow regimes.....	206
7.4.2. Constraints on magma ascent velocity	207

7.4.3. Volcanic hazard consequences	210
7.4.4. Creating eruption scenarios for lava flow hazard mapping	210
7.4.5. Limits of lava flow simulations in volcanic field settings.....	211
7.5. Conclusions	212
Chapter Eight – Discussion and conclusions	217
8.1. Discussion.....	217
8.2. A conceptual model for eruption style susceptibility mapping	218
8.3. A conceptual model for lava flow susceptibility mapping.....	227
8.4. Towards a GIS-based hazard assessment of monogenetic volcanic fields	231
8.5. Conclusions	233
8.5.1 Research objectives.....	233
8.5.2. Future directions of research.....	235
8.5.3. Concluding remarks	237
References cited.....	242
Appendix A – Pullout map.....	283
Appendix B – Supplementary data (DVD)	285
Appendix C – Statement of contribution	301

List of Figures

- Figure 2.1 Simplified geologic and tectonic map of the broader Auckland region, based on Kermode (1992) and Edbrooke (2001). The black rectangle shows the area of the AVF with the locations mentioned in the text (1 – Takapuna Beach, 2 – Cheltenham Beach, 3 – Rangitoto, 4 – Motutapu Island, 5 – Browns Island, 6 – One Tree Hill, 7 – Pukaki maar, 8 – Crater Hill.). The roman numerals show the area of the three domains within the AVF mentioned in the text (I – North Shore, II – Central Auckland, III – Manukau Lowlands). The coordinates are in metres (New Zealand Map Grid). 16
- Figure 2.2 Simplified stratigraphic column with characteristics of the main geologic formations occurring in Auckland. Note that the depth indicated in the sedimentary column varies from region to region. The values used here are based on Edbrooke et al. (1998). Sedimentary characteristics are after Kermode (1992) and Edbrooke et al. (1998). The Dun Mountain–Maitai Terrane has not been penetrated by the drill core described in Edbrooke et al. (1998), but it is inferred to be located underneath Auckland based on magnetic anomalies (e.g. Eccles et al., 2005). 18
- Figure 2.3 Outcropping Waitemata units with an extensive multidirectional fracture system at Takapuna Beach (A) and Cheltenham Beach (B) in the North Shore. For the location map, see Fig. 2.1. 19
- Figure 2.4 Oblique view of the basaltic volcanic regions in Northland and Auckland. The coordinates are in metres (New Zealand Transverse Mercator 2000). 21
- Figure 2.5 (A) Location map for the 52 monogenetic vents scattered around the Auckland region overlain on the LiDAR DSM. (B) Location of the 52 eruptive centres (green triangles) within the City of Auckland overlain on a false-colour multispectral SPOT-5 satellite image. Note that the areas in grey to green are the urban and heavily populated parts of Auckland, while the red colour shows distribution of vegetated areas, such as forest or park. The coordinates are in metres (New Zealand Transverse Mercator 2000). 23
- Figure 2.6 Simple and complex magma generation scenarios based on three examples from the AVF. 24
- Figure 2.7 Examples of monogenetic volcanoes from the AVF. For the locations of these examples, the reader is referred to Fig. 2.5 and Appendix A. (A) Overview photo of monogenetic volcanoes in the Auckland area. (B) An example of a wide and circular crater formed by extensive phreatomagmatic eruptions, Pukaki volcano. (C) Combination of phreatomagmatic eruption and late stage magmatic eruption forming complex monogenetic volcanoes, such as Browns Island in the Waitemata Harbour. (D) Purely magmatic processes form scoria cone and extensive lava flow fields at Rangitoto. 26
- Figure 2.8 Sedimentary structures in tuff deposits formed by phreatomagmatic eruptions in the AVF. For location of these examples, the reader is referred to Fig. 2.5 and Appendix A. (A) Dune- and cross-bedded units with contrasting granulometric characteristics at the Pupuke eruption centre. (B) Close view of an impact sag

- caused by a ballistically ejected basaltic block at Browns Island. (C) Complex sedimentary unit, exposed at the basal parts of Browns Island tuff pyroclastic sequence, revealing the dominant transportation mechanism (e.g. pyroclastic density current and tephra fall) related to the formation of tuff rings. 28
- Figure 2.9 Simplified sedimentary log for deposits of a Strombolian eruption style, exposed at the Rangitoto scoria cone (see Fig. 2.5 for location). This log gives examples for the contrasting styles of ejecta transport on the flanks of a growing scoria cone by grain flow processes (e.g. lapilli-sized scoria fragments) and ballistics (e.g. larger broken or fluidal-shaped blocks/bombs). Modified from Kereszturi and Németh (2012a)..... 29
- Figure 2.10 Spatial intensity maps of the AVF based on the vent locations. The spatial intensity is calculated by (A) symmetric Gaussian kernel after Kereszturi et al. (2012b), and (B) asymmetric elliptic kernel after Bebbington and Cronin (2011). 33
- Figure 3.1 Overview of topographic data used in this study captured at different spatial scales with different coverage and (vertical) accuracy. For more information about these datasets for Auckland, see text. Note that for accuracy assessment purposes, TLS survey points with 0.5 m average point spacing were used in the present accuracy assessment..... 40
- Figure 3.2 Basic survey concepts of RTK GPS, LiDAR, SRTM and ASTER data acquisition and imaging geometry. The figure is not to scale. The inset shows the vertical and horizontal error in topographic survey after Hodgson and Bresnahan (2004). 44
- Figure 3.3 Field photos of the TLS (A) and RTK GPS surveys (B) carried out on the distal segment of a rubbly a'a lava flow near Flax Point, Rangitoto. (C) Perspective view of the TLS point cloud after registration of point from each station. The inset shows the capability of the TLS to resolve detailed features, such as grass (white arrows). Vegetation was removed manually from the point cloud to obtain bare surface points for the DSM..... 50
- Figure 3.4 Structure of data and interpolation from vector-based input data, such as spot heights and contour lines, using (A) Triangulated Irregular Network (TIN) and (B) linear interpolation, implemented in the ILWIS software package. Note that there are two examples provided for comparison to highlight the effect of user-defined horizontal resolution and vertical precision on the resultant DEM. If the horizontal resolution is too large in relation to the average distance between two neighbouring contour lines, a grid cell is created with the average value of the two input contour line elevations. If the vertical precision is too low, then the resultant grid cell might have the same elevation, and consequently a flat grid cell would be created. 52
- Figure 3.5 (A) Overview of topographic data available in Auckland with various spatial resolutions. From the top to the bottom: 2 m LiDAR DSM, 4 m topo50 DEM, 30 m ASTER GDEM, 90 m SRTM DTM. (B) Elevation histograms for each dataset. 55
- Figure 3.6 (A) Scheme of filtering with moving window of a 3×3 and 5×5 kernel. Z_I to Z_{25} are the grid cells. (B) Concept of the resampling in a gridded environment by the nearest neighbour method. During nearest neighbour resampling, no additional

- interpolation takes place. During resampling the grid cell value of the new resolution is the value of the cell located the closest to the new grid cell centre (e.g. Wood, 1996). 57
- Figure 3.7 High accuracy reference topographic data from the Auckland region. (A) Spatial location of geodetic survey marks as red triangles. The light yellow and light green polygons represent the available point cloud data from LiDAR surveys with rural and urban settings, respectively. The green rectangles are the location of the RTK GPS profiles and TLS DSM data. Numbered test sites in green triangles are: 1 – Onepoto, 2 – Rangitoto, 3 – Browns Island, 4 – Panmure Basin, 5 – Pukewairiki, 6 – Mt. Mangere, 7 – Mangere Lagoon, 8 – Pukeiti and Otutataua, 9 – Crater Hill. (B) RTK GPS profiles from Auckland used in this study. (C) Location of the RTK GPS profiles and the TLS survey site on the Rangitoto volcano. On the right hand-side the TLS-based DSM shown here is with spatial resolution of 0.5 m. 60
- Figure 3.8 Overview of the calculation of zero-order derivatives such as area (A), standard deviation of elevation (B), and volumes (C). 63
- Figure 3.9 Overview of the calculation of first-order derivatives, such as slope angle and slope aspect, in 2D and 3D environment. Note that the examples are used here with a linear, unweighted Prewitt filter (Prewitt, 1970). (A) An example for calculating slope angle along a 2D profile. (B) Perspective view of a 3×3 grid cell kernel, which was used to calculate slope angle and aspect by numerical differentiation in (C). 63
- Figure 3.10 Point-based error assessments using the geodetic survey marks. Note that negative and positive values show places where elevation values are underestimated and overestimated, respectively. 66
- Figure 3.11 Profile-based error assessments for the three test sites. The upper row of graphs shows the elevation of different topographic datasets from the Auckland region. The bottom row of graphs shows the error along the control profile. The insets are the error distribution histograms for each topographic dataset. The bins are 1 m for SRTM DTM, ASTER GDEM and topo50 DEM, and 0.05 m for 10 m and 2 m for LiDAR DSMs. 67
- Figure 3.12 Surface-based error assessment based a TLS acquired reference surface on the distal part of the Rangitoto lava flow field. Note the multimodal (arrows) error distributions for the topo50 DEM, ASTER GDEM and SRTM DTMs. These are due to the dominance of under- and overestimation of the real topography. 68
- Figure 3.13 Variability of zero and first derivatives, calculated from the DSM/DTM/DEMs, along the RTK GPS control profiles for three test sites: Browns Island (first column), Pukaki (second column), and Rangitoto (third column). 69
- Figure 3.14 Error in eruptive volume estimations due to resampling and different input data types, including LiDAR DSM 2m (blue), topo50 DEM (orange), ASTER GDEM (yellow) and SRTM DTM (green). For the location of each evaluation site see Fig. 3.7. This graph shows the overall inaccuracy of ASTER and SRTM DTM products in resolving the fine-details of the topography on monogenetic volcanoes. 71

- Figure 3.15 Graph shows two profiles through the youngest volcanic edifice, Rangitoto, with all the available topographic data from Auckland. The summit crater with a diameter of 200 m is not resolved by the coarser topographic data sources, such as SRTM DTM or ASTER GDEM. The surface roughness on a dm-scale is shown in the inset. This example surface is based on the TLS DSM data on the distal parts of Rangitoto a'ā lava flow. The blue line is the LiDAR 2m data, while the black line is the much higher resolution TLS DSM data. 75
- Figure 4.1 Geology of the AVF after Hayward et al. (2011). The whole area shown in this map coincides with the area of City of Auckland. The inset map shows the location of the AVF and other Quaternary basaltic volcanic fields in the North Island, New Zealand. 83
- Figure 4.2 (A) Diagram of the volcano-sedimentary parts of a conceptualised monogenetic volcano for volume estimation. (B) Methods applied for volume estimation from the different volcano parts. The pie charts represent the DRE correction scheme applied in this study. As the first step of the DRE corrections, a proportion of juvenile, non-juvenile (lithics) and interparticle void space in the volcano parts were used (shown as large pie charts). In the second step, the juvenile content left was corrected for vesicularity (shown as smaller pie charts). 85
- Figure 4.3 Outcrop photos of volcanic deposits from the AVF. (A) Photos showing the well to poorly sorted deposits in one of the scoria cones of Three Kings volcanic complex. The inter-particle void space can be large. (B) Contrasts between juvenile-rich and juvenile-poor units exposed in the succession at Browns Island. Note the large diversity of accidental lithic clasts from the underlying Miocene Waitemata sediments, such as sandstone (black horizontal arrows). (C) A typical lava flow surface from the youngest eruption site, Rangitoto. The lava flows in Rangitoto usually range from shelly pahoehoe to rubbly a'ā lava flow morphotypes. The measuring tape is 50 cm long. 89
- Figure 4.4 (A and B) Microphotographs of pyroclastic rocks from the phreatomagmatic ejecta ring of Orakei Basin. S – sideromelane glass shards and T – tachylite glass shards. (C) Point counting results of a typical thin-section from the Browns Island ejecta ring, showing the maximum 35 vol% of juvenile content. The graph is the evaluation plot for the counts. (D) Closer view of two juvenile fragments with contrasting vesicularity. 91
- Figure 4.5 (A) Scan of a scoria hand specimen from the Rangitoto scoria cone. (B) Binary image of the same sample, showing the distribution of vesicles in white. The red box is the area considered in the 2D vesicularity calculations. (C) Field photo of a moderately vesiculated lava flow texture from the lava flow field of Rangitoto. (D) Thresholded binary image showing the distribution of largest vesicularity population. (E) Graph showing the results of density measurements on scoria (n = 48) and lava rock (n = 42) samples from Rangitoto and Browns Island volcanoes. The densities were measured as envelope density by Micrometrics Geo PyC1360 density analyser. Due to the small diameter (i.e. 2 cm in diameter) of the samples measured in the density analyser, these density and vesicularity values are considered as minimum values. The vesicularity is calculated proportional to 2.8 g/cm^3 94

- Figure 4.6 Results of the new DRE eruptive volume estimates for the AVF. (A) The results of minimum estimates, including those volcanic parts where the volumes can be estimated with a relatively high accuracy. (B and C) Overall DRE eruptive volumes change if distal tephra blankets and diatreme volumes are considered. 102
- Figure 4.7 (A) DRE eruptive volume as a function of time during the evolution of the AVF for each estimate. The ages are based on the most likely simulated eruption history based on the probabilistic analysis of Bebbington and Cronin (2011). The ages are simulated based on 1000 Monte Carlo simulations of the existing event-order of the AVF. Therefore, individual volcanoes might have a slightly different order (Bebbington and Cronin, 2011). (B) Number of volcanic events over the evolution of AVF, showing a decreasing trend since 32 ka..... 103
- Figure 4.8 (A) Spatial distribution of volcanic centres formed during the older (blue triangles within the blue polygon) and younger stages (red triangles within the red polygon) in the AVF with the geometric, areal and volumetric characteristics. The blue, red and black crosses are the geometric centre of older, younger stages and the all ($n = 52$) volcanoes from the AVF, respectively. (B) Spatial distribution of eruptive volume per volcanoes (blue dots) scaled by their volumetric size in the AVF, revealing a couple of exceptionally large volcanic centres (black arrows with names). The numbered red arrows show the distribution of those “paired-volcanoes”. These paired-volcanoes could have formed from the same eruptive event, involving a lateral vent migration. Red numbers with arrows are: 1 – Tank Farm and Onepoto, 2 – Mt. Victoria and Mt. Cambia, 3 – Grafton volcano and Auckland Domain, 4 – Purchas Hill and Mt. Wellington, 5 – Mt. Richmond and McLennan Hills, 6 – Styaks Swamp, Green Mt., Otara Hill and Hampton Park, 7 – Mt. Mangere and Mangere Lagoon, 8 – Wiri Mt. and Ash Hill..... 109
- Figure 4.9 Histograms showing the eruptive volumes of each volcano in the AVF (first column), older stage (≥ 40 ka; second column) and younger stage (≤ 40 ka; third column), using bulk (A) and DRE-corrected volumetric data (B). Bin size is 0.01 km^3 on all histograms. Outliers, such as Rangitoto and One Tree Hill, are not shown on the histograms. 110
- Figure 4.10 (A) Distribution of monogenetic volcanics in the broader Auckland region. The black ellipses show the location of Auckland (AVF), South Auckland (SAVF) and Ngatutura (NVF) volcanic fields, with the duration of volcanic activity and distance from location of the recent manifestation of volcanism. For scale, the average spatial extent of a monogenetic volcanic field is given, based on data from Le Corvec et al. (2013c). (B) Age distribution for the monogenetic volcanic eruptions in the last 2.5 My in the broader Auckland region. The K-Ar radiometric ages are from Briggs et al. (1994)..... 113
- Figure 5.1 Eruptive histories (E) of monogenetic volcanoes can be defined as an array of numbers ordered chronologically. The numerical codes include 1 – fire-fountaining, 2 – Strombolian, 3 – violent Strombolian, 4 – phreatomagmatic, 5 – Surtseyan and 6 – magmatic effusive activity. Modified from Kereszturi and Németh (2012a). 128
- Figure 5.2 Area-equivalent circles of Browns Island, calculated from the delimited area of each differentiated eruption style type..... 131
- Figure 5.3 Overview of the AVF and two cross-sections through the Manukau Lowlands. The drill core data are from the PETLAB database (www.pet.gns.cri.nz).

Geographic divisions on the left of the map include: North Shore, which includes areas now occupied by sea water in the Waitemata Harbour; Central Auckland, which encompasses the elevated parts of the Auckland Isthmus; and the Manukau Lowlands including the Manukau Harbour and the alluvial plain areas with the western slopes of the Hunua Range. The size of the green dots is scaled to the eruptive volume of the phreatomagmatic phase (in $\times 10^6 \text{ m}^3$) of past volcanoes. 133

- Figure 5.4 Area-equivalent circles revealing eruptive histories with either increasing (e.g. One Tree Hill) or decreasing (e.g. Crater Hill) footprints of volcanic hazard during the course of the eruptions..... 136
- Figure 5.5 Histogram of area affected by different volcanic processes forming ejecta rings (A), scoria cones (B) and lava flow (C) in the AVF. The bin size is 0.5 km^2 for all histograms. 137
- Figure 5.6 Contribution of different eruption styles to the total eruptive volumes of each volcano in the AVF. The colouring indicates phreatomagmatic (green), magmatic explosive (yellow) and the magmatic effusive volume (red). The chronological order is a simulated event order from Bebbington and Cronin (2011). 137
- Figure 5.7 Ternary diagram for proportional volumes for three types of eruption styles in the AVF, with those affected by phreatomagmatic and Surtseyan eruptions, magmatic explosive eruptions (fire-fountaining and Strombolian types), and magmatic effusive eruptions. The data were normalised to the mean of each eruptive unit. 138
- Figure 5.8 (A) Proportions of single, compound and complex eruptive histories in the AVF, and their dominant eruption styles. (B) Box plot graphs for the area affected (left) and eruptive volumes (right graph) in relation to eruptive histories. The lower quartile (Q_1), median (m), upper quartile (Q_3), and outliers' values are shown. 139
- Figure 5.9 Spatial distributions of single (A), compound (B), and complex eruption histories (C), as well as the number of eruption styles (D) in the AVF..... 140
- Figure 5.10 Scatter graphs of phreatomagmatic vent-opening volumes of the AVF's volcanoes in relation to the (A) thickness of post-Waitemata non-volcanic sediments, (B) pre-eruptive elevation, (C) distance from the present coastline, and (D) distance from known fault lines. 141
- Figure 5.11 Box plots showing the three sub-areas of the AVF and the total AVF in relation to (A) thickness of post-Waitemata non-volcanic sediments, (B) pre-eruptive elevation, (C) distance from the present coastline, and (D) distance from known fault lines. Note that in graph A, the thickness is inferred to be $\leq 5 \text{ m}$ under volcanoes in the Central Auckland region. 142
- Figure 5.12 Box plots showing the distance from the coast to the volcanoes from three distinct sub-areas of the AVF and the total field in relation to (A) a sea level higher than the present day by 10 m, and (B) 5 m, as well as (C) a sea level lower than the present day by 5 m and (D) by 10 m. 143
- Figure 5.13 A model for internal (red circles) and external (green circles) factors influencing eruption styles in the AVF. Future hypothesised eruption site examples are shown as black dots with the four environmental factors (d_{sea} – distance from sea; d_{fault} – distance from known fault lines; Z_{topo} – topographic

- position, as well as h_{wat} – thickness of water-bearing units). The significance of each environmental factor varies between parts of the field, and there is no sole controlling factor for eruption styles and histories. The listed external environmental factors are in the order of inferred importance. Note the excavation depth of the maar volcanoes is not constrained well, but it is inferred to be very shallow, 50-100 m (Cassidy et al., 2007; Agustin-Flores et al., 2014). The fault location data are after Kenny et al. (2012)..... 146
- Figure 5.14 The relationship between thickness of post-Waitemata non-volcanic sediments and the eruptive volumes of ejecta rings and crater infills for all volcanoes in the Manukau Lowlands (A), and with the largest volume volcanoes of the area (B). Note that all volcanoes located under the predicted line have extremely small erupted volumes, with large extents of anthropogenic modification..... 148
- Figure 6.1 (A) An overview LiDAR-based DSM of the Auckland region with the location of studied volcanic centres. Note that a phreatomagmatic maar volcano, Orakei Basin, and a complex monogenetic volcano with initial phreatomagmatic and late magmatic stage, Crater Hill, both mentioned in the text, are indicated by the dashed arrows. The dashed ellipsoid shows the extent of the Auckland Volcanic Field (after Spörli and Eastwood, 1997). The coordinates are given in New Zealand Transverse Mercator (NZTM2000). The solid boxes indicate the location of Figs. 6.3, 6.4 and 6.8. (B) Location of the 52 eruptive centres (green triangles) within the AVF overlaid on a false-colour multispectral SPOT-5 satellite image. Note that the areas in grey to green are the urban and heavily populated parts of Auckland, while the red colour shows distribution of vegetated areas, such as forest or park. 156
- Figure 6.2 Flow diagram for input data, data processing and results 159
- Figure 6.3 Perspective (A) and profile (B) views of morphometric parameters of lava flows applied in this paper visualised on the Mt. Mangere volcano (for the detailed location see Fig. 6.1)..... 161
- Figure 6.4 Definitions of susceptibility zones (sea, depressions, low-lying area, buffer and ridges/peaks) identified in the AVF visualised on an area from North Shore (for the detailed location see Fig. 6.1). The largest depression in the figure is the Lake Pupuke, generated by series of phreatomagmatic eruptions..... 163
- Figure 6.5 Field photographs illustrating examples of preserved lava flow surfaces and their source scoria cones (black arrows). (A) A’a lava flow surface preserved in the coastal area of Browns Island. (B) Pahoehoe surface related to the Mt. Mangere scoria cone. (C) Fresh a’a lava flow from the youngest eruption centre, Rangitoto. (D) Overview photo of the Mt. Wellington scoria cone and its basaltic lava flow exposed due to extensive quarrying. Note that the white arrow indicates the direction of the lava flow..... 169
- Figure 6.6 Graphs of the main morphometric parameters of lava flows. Age estimates are from Bebbington and Cronin (2011). Note that the black arrows indicate the morphometric values of Rangitoto volcano. 170
- Figure 6.7 Figure showing the spatial density of the entire field (green background on each map) based on the location of the 50 eruption centres (triangles in A). A 400 m wide zone at the coastline is indicated by black-grey-white lines, see text for

- explanation. (A) Watershed ranking based on the averaged kernel density. The contour lines (black lines) represent the 25%, 50% and 75% percentage of input point used to estimate the probability density distribution. (B) Watershed ranking based on cumulative bulk volume. (C and D) These two maps show the area portion (pie diagrams) of zones within watersheds for the Scenario 1 (C) and Scenario 2 (D). The colouring of the watershed boundaries shows the ratio between the total areas of buffer (light green) and ridge/peaks (dark green) as well as depressions (red) and low-lying areas (pink). The colours used here are the same as on the lava flow susceptibility map in Fig. 6.9..... 177
- Figure 6.8 Cross-section through the central, elevated part, of the AVF, illustrating the channelised lava flows by valley eroded into the Waitemata sandstone. For the detailed location see Fig. 6.1. 180
- Figure 6.9 Lava flow susceptibility map based on Scenario 1 (without Rangitoto) for the AVF showing the susceptibility zones with the major hydrological and topographical characteristics (A) and with major infrastructures (B). 182
- Figure 7.1 Overview of the AVF and its volcanoes (black dots) and the location of the simulated lava flows (numbered black dots). 193
- Figure 7.2 Graph shows three effusion curves of Little Rangitoto (A), Mt. Roskill (B) and Three Kings (C) and their comparison (D). 199
- Figure 7.3 Lava flow simulation results of Little Rangitoto (left-hand side) and comparison with the mapped extent of the flow (right-hand side). On the left-hand side, the histogram insets show the distribution of thickness values for the simulations. 201
- Figure 7.4 Lava flow simulation results of Mt. Roskill (left-hand side) and comparison with the mapped extent of the flow (right-hand side). On the left-hand side, the histogram insets show the distribution of thickness values for the simulations; the smaller histograms are the original flow thickness distributions. 202
- Figure 7.5 Lava flow simulation results of Three Kings (left-hand side) and comparison with the mapped extent of the flow (right-hand side). On the left-hand side, the histogram insets show the distribution of thickness values for the simulations; the smaller histograms are the original flow thickness distributions. 203
- Figure 7.6 Dyke widths as a function of ascent velocity for a fissure length of 50, 100 and 150 m. The magma flux is estimated at $40 \text{ m}^3/\text{s}$, in accordance with the value of best simulation. 207
- Figure 7.7 Envisaged feeder dyke geometries of the three eruption centres. Abbreviated parameters are U – ascent velocity, L – flow length, F – fissure length, and V – bulk eruptive volume. 209
- Figure 8.1 Classified maps of features used for eruption style susceptibility mapping in the AVF. (A) Combined thickness map of post-Waitemata uncompact non-volcanic sediments. (B) Topographic elevation. (C) Distance from the present shore line, (D) Distance from known faults. 220
- Figure 8.2 Susceptibility map (red = high, green = low) for phreatomagmatic vent-opening phase in future eruptions in the AVF, based on combining the maps shown in Fig. 8.1. The inset shows the distribution of each susceptibility class. The areas below sea level (white) were not considered. 222

- Figure 8.3: Scatter graph showing the relationship between susceptibility classes for phreatomagmatic eruptions (Fig. 8.2) and the median volume estimated from the interpolated raster of phreatomagmatic phases. 224
- Figure 8.4 Eruption sequence forecast map based on the eruption style susceptibility map (Fig. 8.2) and interpolated values of the phreatomagmatic volumes of the 52 volcanoes in the AVF. The likely eruption sequences and eruptive volume percentages (blue column = phreatomagmatic volume; light yellow column = magmatic explosive and effusive volume) of three example volcanoes are shown for a magma supply of $8 \times 10^6 \text{ m}^3$ (e.g. Panmure Basin; Chapter 4). 225
- Figure 8.5 A model of proximal and distal zones in lava flow simulations in a monogenetic volcanic field setting. A hypothetical vent (red dot) is characterised by a radius (r), which is 1 km here. The circle with radius r shows the potential area that might be modified by initial cratering and ejecta ring formation during a phreatomagmatic eruption. This might be coupled with an eruption taking place on a watershed boundary (e.g. Mt. Albert). Lava flow modelling within proximal areas thus has a higher degree of uncertainty. Accuracy of prediction of potential lava flow path and length increases towards distal zones, where topographic modification from the eruption is not extensive. 228
- Figure 8.6 Maps showing different methods of modelling lava flow susceptibility in the North Shore area, including (A) stochastic lava flow inundation map from a hypothesised vent (blue triangle), and (B) thickness map simulated by MAGFLOW using the Mt. Roskill effusive curve and magma supply volumes (e.g. Chapter 7). The insets shown in (B) are topographic profiles with the simulated lava flows (under red curve). The valley-confined (C) and unconfined (UC) flow zones of each simulation are marked. 230
- Figure 8.7 Structure of spatial attribute based hazard assessment designed for the AVF. The layers of the database can be separated into input (I), hazard (H) and risk (R) components. 232

List of Tables

Table 2.1 Summary of simulated ages (from Bebbington and Cronin, 2011; 2012), eruption styles (from Hayward et al., 2011) and eruptive volumes (from Allen and Smith, 1994) of the AVF volcanoes.	32
Table 3.1 Results of the error assessment of the topographic data for Auckland.	65
Table 4.1 Summary of physical properties used to establish the input data for DRE corrections.	98
Table 4.2 Summary of the DRE correction values used in this study.	100
Table 4.3 Summary of DRE-corrected, minimum eruptive volumes estimate for each monogenetic volcano in the AVF. The underlined eruptive volumes are based on the bulk volume data published in Allen and Smith (1994), recalculated with our DRE correction scheme. The chronology shown here is based on simulated ages adapted from Bebbington and Cronin (2011). Notes: 1 – Pupuke and North Head bulk volumes was corrected for a higher amount of juvenile contents (Allen and Smith, 1994), 2 – In the case of Maungataketake, the bulk ejecta rings volume has been corrected for erosion, 3 – Bulk lava flow volumes has been updated since Kereszturi et al. (2012b) due to more information about the pre-eruptive surface, 4 – The bulk volume for St. John volcano is estimated using the inferred areal extent of the flow and a constant thickness of 10 m, 5 – The bulk volume of McLaughlin Mt. includes the bulk volume of the three small, Puhinui craters’ as well, 6 – Lava flow from Mt. Eden and Three Kings flowed partially on top of one of the earliest lava flows of Central Auckland are from the St. John volcano (Eade, 2009). As a result of this stratigraphy, the area proportional bulk volume of St. John lava flow has been substrate from the bulk volumes of Mt. Eden and Three Kings volcanoes, 7 – Mt. Eden’s bulk volume contains the ejecta ring and magmatic crater infill of Te Pou Hawaiki volcano (Fig. 4.1), 8 – In the case of Mt. Mangere 0 m a.s.l. plane were used as the pre-eruptive surface, however, it is possible that the contact between lava flow and the Tauranga Formation is a couple of m below the present sea-stand. Therefore, this is a minimum volume, 9 – The initial phreatomagmatic phase of Rangitoto is approximated using a volume of a crater with diameter of 800 m and depth of 30 m, as well as the ejecta rings volume equivalent to the Panmure Basin. The selection of this approximation was based on the available geophysical surveys of Rangitoto, after Milligan (1977), 10 – Note that the bulk volume estimate for Rangitoto contains the eruptive products from both phase of activities.	104
Table 4.4 Summary of field-scale and edifice-scale characteristics of the AVF for the older (250–40 ka) and younger (<40 ka) stages and for the whole field. The duration is based on an average of 10 m ³ /s eruption rate. Note: ph – phreatomagmatic eruptions, mag – magmatic explosive eruptions, eff – effusive activity.	114
Table 5.1 Summary of the DRE-corrected eruptive volumes and eruption styles inferred from the pyroclastic deposits preserved at each monogenetic volcano in the AVF. The chronology shown here is based on simulated ages adapted from Bebbington and Cronin (2011). The underlined eruptive volumes are based on the bulk	

volume data published in Allen and Smith (1994), recalculated with our DRE correction scheme (Chapter 4). Key: “L” – sub-region within the AVF in which “N” is North Shore, “C” is Central Auckland and “M” is Manukau Lowlands; “ph.” – phreatomagmatic phase; “mag.” – magmatic explosive phase; “eff.” – magmatic effusive phase; “E” – refers to eruption history or eruption sequence with the eruption styles as 1 – phreatomagmatic, 2 – magmatic explosive, 3 – magmatic effusive; “ T_{sed} ” – thickness of the post-Waitemata non-volcanic sediments; “ d_{sea} ” – distance from coastline; “+10 m” and “+5m” – distance from the coastline in the case of a higher sea level by 10 m and 5 m respectively; “pr. day” – distance from the present day coastline; “-10 m” and “-5m” – distance from the coastline in the case of a lower sea level by 10 m and 5 m respectively; “ Z_{topo} ” – elevation of pre-eruptive topography at vent location, in which zero indicates that the vent is on the shore or submarine; “ d_{fault} ” – distance from known fault line..... 124

Table 6.1 Summary of morphometric parameters for the studied fifteen lava flows. Z – is the pre-eruptive basement elevation in meter a.s.l. that was used in the bulk volume calculations.	165
Table 6.2 Differences in the area of hazard zones using two simulated scenarios.....	172
Table 6.3 Properties of large (larger than 2 km ²) watersheds. The values in bold represent either the smaller topographical differences between catchment rims and drainage than a lava flow with average thickness or those catchment that are limited (i.e. smaller than average lava flow) in volume capacities.....	174
Table 7.1 Summary of the input physical parameters of the lava flows (L_{max} – maximum length, A_{lava} – area, T_{max} and T_{mean} – maximum and average thickness, bulk and DRE-corrected eruptive volumes).	194
Table 7.2 Overview of MAGFLOW input parameters for the simulation in the AVF.	197
Table 7.3 Comparison of properties of simulated lava flow scenarios of Little Rangitoto, Mt. Roskill and Three Kings examples. The best-fit scenarios are highlighted in green.	204
Table 8.1 List of cities and infrastructure located on or near monogenetic volcanic fields. In such settings susceptibility mapping could be useful to improve hazard assessment. Key: M – monogenetic; P – polygenetic; pop. – population (in million) in the metropolitan area; VF – volcanic field.....	226

